Applied Physics Letters

Thickness dependence of dielectric constant of alumina films based on first-principles calculations

Cite as: Appl. Phys. Lett. **121**, 062902 (2022); https://doi.org/10.1063/5.0106721
Submitted: 29 June 2022 • Accepted: 26 July 2022 • Published Online: 12 August 2022

Shogo Fukushima, Rajiv K. Kalia, Aiichiro Nakano, et al.

© 2022 Author(s).

Thickness dependence of dielectric constant of alumina films based on first-principles calculations

Cite as: Appl. Phys. Lett. **121**, 062902 (2022); doi: 10.1063/5.0106721
Submitted: 29 June 2022 · Accepted: 26 July 2022 ·
Published Online: 12 August 2022

View Online

Export Citation

CrossMark

Shogo Fukushima,[1,2] Rajiv K. Kalia,[2] Aiichiro Nakano,[2,a)] Fuyuki Shimojo,[1] and Priya Vashishta[2]

AFFILIATIONS

[1]Department of Physics, Kumamoto University, Kumamoto 860-8555, Japan

[2]Collaboratory for Advanced Computing and Simulations, Department of Physics and Astronomy, Department of Computer Science, Department of Chemical Engineering and Materials Science, Department of Quantitative and Computational Biology, University of Southern California, Los Angeles, California 90089-0242, USA

[a)]Author to whom correspondence should be addressed: anakano@usc.edu

ABSTRACT

Optoelectronic properties of devices made of two-dimensional materials depend largely on the dielectric constant and thickness of a substrate. To systematically investigate the thickness dependence of dielectric constant from first principles, we have implemented a double-cell method based on a theoretical framework by Martyna and Tuckerman [J. Chem. Phys. **110**, 2810 (1999)] and therewith developed a general and robust procedure to calculate dielectric constants of slab systems from electric displacement and electric field, which is free from material-specific adjustable parameters. We have applied the procedure to a prototypical substrate, Al_2O_3, thereby computing high-frequency and static dielectric constants of a finite slab as a function of the number of crystalline unit-cell layers. We find that two and four layers are sufficient for the high-frequency and static dielectric constants of (0001) Al_2O_3 slabs to recover 90% of the respective bulk values computed by a Berry-phase method. This method allows one to estimate the thickness dependence of dielectric constants for various materials used in emerging two-dimensional nanophotonics, while providing an analytic formula that can be incorporated into photonics simulations.

Published under an exclusive license by AIP Publishing. https://doi.org/10.1063/5.0106721

Dielectric screening by a substrate significantly modifies optoelectronic properties of devices made of two-dimensional (2D) materials deposited on it. Qiu *et al.* reported that the optoelectronic properties of few-layer black phosphorus on a substrate are sensitive to the species of the substrate such as sapphire (Al_2O_3) and hexagonal boron nitride (hBN).[1] Optoelectronic properties, such as quasiparticle gap, optical gap, and exciton binding energy, are largely influenced by dielectric properties and surface structures of the substrates. In transition metal dichalcogenides (TMDs), it is well known that additional screening from a metallic graphene substrate or capping layer can reduce the quasiparticle bandgap. Bradley *et al.* reported that direct and indirect band gaps of few-layer $MoSe_2$ can be reduced by 0.1–0.2 eV by additional bilayer graphene on a 6H–SiC(0001) substrate.[2] Raja *et al.* investigated the effects of graphene on dielectric constants and bandgaps of WS_2 and WSe_2 on SiO_2 and hBN substrates.[3] They also reported that additional bilayer graphene reduces the bandgap by 0.13 eV. Such substrate screening should play a dominant role in emerging nanophotonics based on 2D materials.[4,5] In these applications, it is essential to accurately assess the dielectric constant of substrate as a function of its thickness, because dielectric constant of a finite slab often exhibits highly nontrivial thickness dependence.[6]

In the literature, several methods have been suggested for calculating dielectric constants of atomically thin 2D materials. Laturia *et al.* calculated dielectric constants of 2D materials such as hBN and TMDs from the principle of equivalent capacitance, using a dielectric constant of supercell computed from Born effective-charge tensor and force-constant matrix.[7] Santos *et al.* suggested a method for calculating dielectric constants of slabs, by introducing a compensating electric field in vacuum area between polarized slabs due to periodic boundary condition.[8] They calculated dielectric constants of few-layer MoS_2 under a finite electric field. In these methods, corrections were made to incorporate the effects of a vacuum layer on dielectric constant caused by periodic boundary conditions. However, it remains untested for thicker slabs whether these corrections can adequately eliminate

Coulomb interaction between periodic images. Instead, we here focus on a general theoretical framework by Martyna and Tuckerman to explicitly eliminate Coulomb interaction between periodic images.[9–11] They applied the framework to cluster (0D),[9] wire (1D),[10] and slab (2D) systems.[11] In their 2D method, long-range Coulomb interaction along the direction perpendicular to 2D surface is excluded in the Ewald summation. Hereafter, we call this method "double-cell method" because two types of supercells are used for the calculation of wave functions and long-range Coulombic interaction, respectively.[12] Another serious problem is the sensitivity to material-specific adjustable parameters used to define the boundary between material and vacuum in existing methods. We have developed a simple method to calculate dielectric constants of slab systems from electric displacement and electric field, which is free from material-specific adjustable parameters. Accordingly, the method is generally applicable to other materials without any modification and robust, e.g., with respect to the presence of defects.

In this paper, we apply the double-cell method to a prototypical dielectric substrate, Al_2O_3, which is used widely, e.g., as substrate for femtosecond surface x-ray scattering of WSe_2,[13] sol–gel preparation of TiO_2 film,[14] room-temperature ferromagnetism of In_2O_3,[15] and metal-organic vapor-phase epitaxial growth of ZnO nanorods.[16] We calculate high-frequency and static dielectric constants of Al_2O_3 slabs and investigate their thickness dependence and convergence toward the respective bulk values, which, in turn, are computed using a Berry-phase method.[17,18] This paper describes step-by-step procedures that we have developed for computing thickness-dependent dielectric constants of slab systems based on the double-cell method and compares their computational efficiency with previously proposed methods. Moreover, we provide analytical formula that can be used in photonic simulations of thin slabs[19] such as increasingly available freestanding films.[20,21]

As a reference, we first compute dielectric constants in bulk system, for which several methods have been proposed.[17,18,22,23] In this study, we use the method proposed by Umari *et al.* for the treatment of homogeneous electric field within first principles calculations.[17,18] Generally, dielectric constant ε_ω depends on the frequency ω of the external electric field. For ω above the largest phonon frequency, we compute the high-frequency dielectric constant ε_∞ including only electronic response. The ε_∞ is calculated as

$$\varepsilon_\infty = 1 + 4\pi\frac{\Delta P_E}{E}, \quad (1)$$

where ΔP_E is the change in polarization defined by Resta *et al.*[24] due to the finite electric field E for fixed atomic positions. In addition, we compute the static dielectric constant ε_0, which includes both electronic and ionic responses. To include the ionic response, we take into account of atomic relaxation by performing structure optimization under the finite electric field. The ε_0 can then be obtained by including ionic contribution in ΔP_E.

Ewald method is commonly employed in the calculation of long-range Coulombic interaction when using periodic boundary condition. In order to exclude Coulomb interaction between periodic images, Martyna and Tuckerman suggested methods for calculating Coulomb energy if one or more dimensions are non-periodic.[9–11] In their method, two types of supercells are used, i.e., a small cell to calculate the short-range energy contribution in the Ewald method as well as wave functions and electron density and a larger cell to evaluate the long-range energy contribution that excludes periodic-image artifact.[12] In this study, we used this "double-cell method" to investigate dielectric properties of slab systems. The detailed description of the calculation method is provided in the supplementary material.

Dielectric constant is defined as the ratio between electric displacement D and electric field E. We obtain dielectric constants of slab systems by applying an external electric field E_{ext} and calculating D and E from local Kohn–-Sham (KS) potential $V_{loc}(z)$ along [0001] direction. Figure 1 shows the difference of $V_{loc}(z)$ with and without the electric field for a slab of one-crystalline-unit-cell thickness

$$\Delta V^E_{loc}(z) = V^E_{loc}(z) - V^0_{loc}(z), \quad (2)$$

where $V^E_{loc}(z)$ and $V^0_{loc}(z)$ are the local KS potentials under finite electric field E and zero electric field, respectively. Red and blue lines in Fig. 1 represent $\Delta V^E_{loc}(z)$ without and with atomic relaxation, which correspond to ε_∞ and ε_0, respectively. Compared to vacuum ($0\,Å < z < 5\,Å$, $20\,Å < z < 25\,Å$), smaller slopes are observed in slab ($5\,Å < z < 20\,Å$) due to screening. D and E are calculated from the slope of $\Delta V^E_{loc}(z)$ by linear fitting in vacuum and slab regions, respectively. We then calculate the dielectric constant as D/E. While an alternative method to determine the dielectric constant would use polarizations calculated by the double-cell method, which was found to be less effective (see the supplementary material).

The electronic states are calculated using the projector augmented-wave (PAW) method[25,26] within the framework of a density functional theory (DFT). Projector functions are generated for the 3*s* and 3*p* states of aluminum (Al) and 2*s* and 2*p* states of oxygen (O). The generalized gradient approximation (GGA) is used for the exchange-correlation energy.[27] The momentum-space formalism was utilized, where the plane wave cutoff energies are 30 and 250 Ry for the electronic pseudo-wave functions and pseudo-charge density, respectively. $3 \times 3 \times 1$ k points are used for Brillouin-zone sampling for electronic-structure calculations in the slab system, with 3×3 k points in the lateral directions. An external electric field of $E_{ext} = 10^{-3}$ a.u. is applied, which is within the linear-response range (see the supplementary material). To investigate the dependence of ε_∞ and ε_0 on the number of layers n, we use the bulk system and slab system consisting of 1, 2, 3, 4, and 5 layers (referred to as 1L, 2L, 3L, 4L, and 5L systems) of the Al_2O_3 slab, as shown in Fig. 2, where the surface-normal (z) direction is the crystallographic [0001] direction. The bulk system containing 120 atoms in an orthorhombic supercell is used with periodic boundary condition. The orthorhombic supercell size is

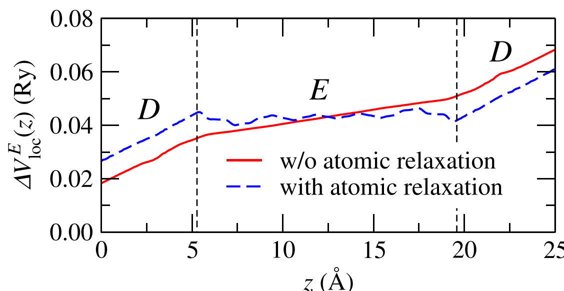

FIG. 1. Differences of local Kohn–Sham potential of a one-layer system with and without the electric field. Red and blue lines represent $\Delta V^E_{loc}(z)$ without and with atomic relaxation, respectively.

Published under an exclusive license by AIP Publishing

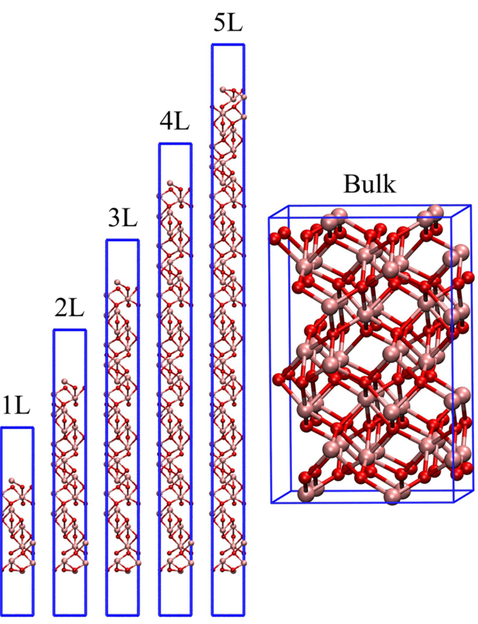

FIG. 2. Schematic of the simulation systems of Al_2O_3. Magenta and red spheres represent Al and O atoms, respectively, while blue lines represent edges of the simulation supercell.

$9.668 \times 8.416 \times 13.189$ Å^3. The 1L, 2L, 3L, 4L, and 5L slab systems containing 30, 60, 90, 120, and 150 atoms in a hexagonal supercell are used. The hexagonal 1L, 2L, 3L, 4L, and 5L supercells are set to be $4.900 \times 4.900 \times 25$, $4.878 \times 4.878 \times 37.5$, $4.861 \times 4.861 \times 50$, $4.856 \times 4.856 \times 62.5$, and $4.852 \times 4.852 \times 75$ Å^3, respectively. These supercell sizes in x and y directions are decided so that the pressure becomes 0 GPa and that of z direction is decided by inserting vacuum regions of 5 Å in top and bottom of supercell in the z direction. Conventional periodic boundary conditions are used in x and y directions in the slab systems.

We first calculate the high-frequency and static dielectric constants, ε_∞ and ε_0, of the bulk system in three (x, y, and z) directions. It is known that dielectric properties of Al_2O_3 are anisotropic between vertical ($\perp$) and parallel ($\|$) directions to [0001].[28] ε_∞ and ε_0 vertical to [0001] are calculated by the average of x and y directions. Table I shows the obtained ε_∞ and ε_0 in the present work, which are in good agreement with the previous work by Schubert *et al.*[29] These values should coincide with ε_∞ and ε_0 of slabs in the infinite-thickness limit.

As mentioned previously, dielectric constants are calculated by the ratio of D and E obtained from the slopes of $\Delta V^E_{\mathrm{loc}}(z)$ in vacuum and slab, respectively. However, the dielectric constants, in particular, ε_0, depend sensitively on the range of linear-fitting w due to the fluctuation of $\Delta V^E_{\mathrm{loc}}(z)$ in slab and accordingly the estimated E value (see the blue line in Fig. 1). On the other hand, D obtained by linear fitting is insensitive to w and is almost the same as E_{ext}, as expected. Figure 3 shows ε_∞ and ε_0 as a function of w, while the center of the range of the linear fitting is fixed at the center of the slab. Fluctuations of ε_∞ are sufficiently small for all systems, while those of ε_0 are larger. In particular, fluctuation of ε_0 for 1L system is too large to determine a unique value, whereas those for 2, 3, 4, and 5L systems converge as w increases. For statistical estimation while excluding the effects of surface, the dielectric constants and their error bars are obtained from the average and standard deviation at $50\% < w/d_n^{\mathrm{slab}} < 80\%$, where d_n^{slab} is the thickness of the n-layer slab system.

TABLE I. High-frequency and static dielectric constants of Al_2O_3.

		Schubert *et al.*[29]	Present work
$E \perp [0001]$	ε_∞	3.077	2.937
	ε_0	9.385 ± 0.013	9.561
$E \parallel [0001]$	ε_∞	3.072	3.061
	ε_0	11.61 ± 0.016	11.86

Figure 4 shows the calculated ε_∞ and ε_0 as a function of n. 1L system is an outlier, since the statistical errors of ε_∞ and ε_0 of are much larger than those of the other systems. On the other hand, ε_∞ and ε_0 of 2, 3, 4, and 5L systems monotonically increase as a function of n. Convergence to the bulk value can be fitted to the following analytical formula:

$$\varepsilon_\infty = \varepsilon^{\mathrm{bulk}}_{\infty,\,[0001]} - \frac{a}{n+b}, \tag{3}$$

$$\varepsilon_0 = \varepsilon^{\mathrm{bulk}}_{0,[0001]} - \frac{c}{n+d}, \tag{4}$$

where $\varepsilon^{\mathrm{bulk}}_{\infty,\,[0001]}$ and $\varepsilon^{\mathrm{bulk}}_{0,\,[0001]}$ are the high-frequency and static dielectric constants of bulk in [0001] direction, whereas a, b, c, and d are fitting parameters ($a = 7.241$, $b = 33.39$, $c = 9.165$, and $d = 3.679$). The fit reasonably describes the n-dependence of ε_∞ and ε_0, which converges to respective bulk values. According to these thickness dependences, ε_∞ and ε_0 of the slab system have exceeded 90% of the corresponding bulk values at 2 and 4 layers, respectively. These thickness dependences allow us to estimate the dielectric constants of finite-layered alumina and predict their effects on optoelectronic properties when it is used as a substrate. Thickness dependence was observed experimentally for the dielectric constant of alumina films.[30,31] While commonly observed dielectric constant values increase with the thickness of the

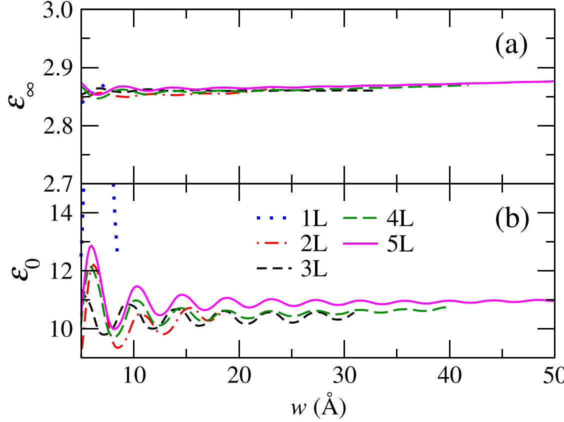

FIG. 3. (a) High-frequency and (b) static dielectric constants as a function of the range w of linear fitting. Blue, red, black, green, and magenta lines represent the dielectric constants of 1, 2, 3, 4, and 5L systems, respectively.

Published under an exclusive license by AIP Publishing

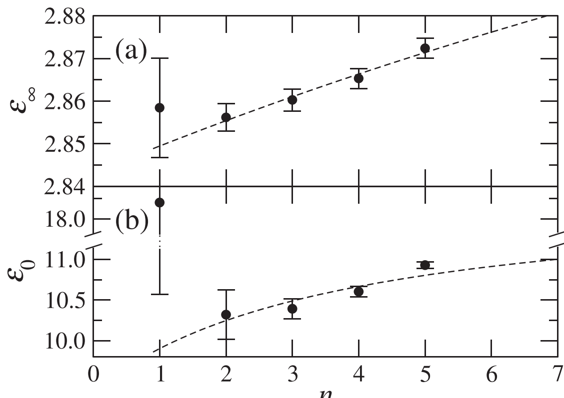

FIG. 4. (a) High-frequency and (b) static dielectric constants as a function of the number of layers n. Dashed lines show the best fits [Eqs. (3) and (4)].

Al_2O_3 film down to 200 Å,[30] a previous study reported a dielectric constant ($\varepsilon_0 \sim 11$) for thin (10–50 Å) Al_2O_3 atomic layer deposition (ALD) films.[32] Nevertheless, it is experimentally highly challenging to measure the dielectric constant of isolated thin slabs without substrate effects. In addition, thin Al_2O_3 films in experiments are usually amorphous, and it is reported that the dielectric constant of amorphous Al_2O_3 (∼8.0) is lower than the crystalline value (∼12.0).[33] Because we consider perfect crystalline slab, the calculated values tend to be higher than experimental values on amorphous ALD films.

Experimentally, dielectric constants of ultrathin alumina films are affected by contacts with other materials.[30,34] Such interfacial systems can have defects and varying coordination numbers.[35] We have thus investigated effects of surface defects on dielectric constants. The calculated $\Delta V_{\rm loc}^{E}(z)$ with oxygen vacancies are nearly the same as those of perfect structures as shown in Fig. S5 in the supplementary material. These results confirm that the proposed method is robust with respect to the presence of defects.

Finally, we compare the computational efficiency and robustness of the proposed method with those of previously suggested methods. We first examine supercell-size dependence of ε_0 calculated based on an alternative method proposed by Santos *et al.*[8] (see Fig. S1 in the supplementary material). However, the calculated ε_0 depends significantly on the supercell size, especially for thin slabs. This is contrary to the double-cell method proposed in this work, which gives supercell size-independent polarization of an isolated slab without the use of excessively large supercells, as shown in Fig. S2. We have also tested an alternative method to calculate the thickness dependence of ε_0 through polarization using Eq. (1), but it produces incorrect behavior as shown in Fig. S3. These comparisons with alternative methods to calculate dielectric constants confirm the computational efficiency and robustness of our method.

In summary, we have developed a robust procedure to determine thickness-dependent dielectric constants of slabs from first principles based on a double-cell method and applied it to Al_2O_3. The calculated high-frequency and static dielectric constants as a function of the number of layers monotonically converge to respective bulk values computed by the Berry-phase method. It was estimated that 2 and 4 layers are sufficient, respectively, for the high-frequency and static dielectric constants to recover 90% of bulk values. We have also provided accurate analytical formula, Eqs. (3) and (4), which can be used in photonic simulations of thin slabs.

See the supplementary material for detailed descriptions of Berry-phase and double-cell methods, comparison with alternative calculation methods in Figs. S1–S3, linear dependence on the electric field in Fig. S4, and the effects of surface defects on dielectric constant in Fig. S5.

This study was supported by JSPS KAKENHI (Grant Nos. 21J10836 and 21H01766) and JST CREST (Grant No. JPMJCR18I2), Japan. The work at the University of Southern California was supported by the National Science Foundation, Future Manufacturing Program (Award No. NSF 2036359). The authors thank the Supercomputer Center, the Institute for Solid State Physics, University of Tokyo, for the use of the facilities. The computations in this work were also performed using the facilities of the Research Institute for Information Technology, Kyushu University.

AUTHOR DECLARATIONS

Conflict of Interest

The authors have no conflicts to disclose.

Author Contributions

Shogo Fukushima: Conceptualization (equal); Funding acquisition (equal); Investigation (equal); Supervision (equal); Validation (equal); Visualization (equal); Writing – original draft (equal); Writing – review and editing (equal). **Rajiv K. Kalia:** Funding acquisition (equal); Investigation (equal); Resources (equal); Validation (equal); Visualization (equal); Writing – original draft (equal); Writing – review and editing (equal). **Aiichiro Nakano:** Conceptualization (equal); Funding acquisition (equal); Resources (equal); Supervision (equal); Writing – original draft (equal); Writing – review and editing (equal). **Fuyuki Shimojo:** Conceptualization (equal); Methodology (equal); Software (equal); Supervision (equal); Writing – original draft (equal); Writing – review and editing (equal). **Priya Vashishta:** Project administration (equal); Writing – original draft (equal); Writing – review and editing (equal).

DATA AVAILABILITY

The data that support the findings of this study are available from the corresponding author upon reasonable request.

REFERENCES

[1] D. Y. Qiu, F. H. da Jornada, and S. G. Louie, Nano Lett. **17**(8), 4706 (2017).
[2] A. J. Bradley, M. M. Ugeda, F. H. da Jornada, D. Y. Qiu, W. Ruan, Y. Zhang, S. Wickenburg, A. Riss, J. Lu, S. K. Mo, Z. Hussain, Z. X. Shen, S. G. Louie, and M. F. Crommie, Nano. Lett. **15**(4), 2594 (2015).
[3] A. Raja, A. Chaves, J. Yu, G. Arefe, H. M. Hill, A. F. Rigosi, T. C. Berkelbach, P. Nagler, C. Schuller, T. Korn, C. Nuckolls, J. Hone, L. E. Brus, T. F. Heinz, D. R. Reichman, and A. Chernikov, Nat. Commun. **8**, 15251 (2017).
[4] A. B. Khanikaev and G. Shvets, Nat. Photonics **11**(12), 763 (2017).
[5] M. Turunen, M. Brotons-Gisbert, Y. Dai, Y. Wang, E. Scerri, C. Bonato, K. D. Jöns, Z. Sun, and B. D. Gerardot, Nat. Rev. Phys. **4**(4), 219 (2022).
[6] M. Stengel and N. A. Spaldin, Nature **443**(7112), 679 (2006).
[7] A. Laturia, M. L. Van de Put, and W. G. Vandenberghe, npj 2D Mater. Appl. **2**(1), 6 (2018).
[8] E. J. G. Santos and E. Kaxiras, ACS Nano **7**(12), 10741 (2013).

Published under an exclusive license by AIP Publishing

[9]G. J. Martyna and M. E. Tuckerman, J. Chem. Phys. **110**(6), 2810 (1999).
[10]P. Minary, J. A. Morrone, D. A. Yarne, M. E. Tuckerman, and G. J. Martyna, J. Chem. Phys. **121**(23), 11949 (2004).
[11]P. Mináry, M. E. Tuckerman, K. A. Pihakari, and G. J. Martyna, J. Chem. Phys. **116**(13), 5351 (2002).
[12]D. A. Yarne, M. E. Tuckerman, and G. J. Martyna, J. Chem. Phys. **115**(8), 3531 (2001).
[13]I. C. Tung, A. Krishnamoorthy, S. Sadasivam, H. Zhou, Q. Zhang, K. L. Seyler, G. Clark, E. M. Mannebach, C. Nyby, F. Ernst, D. Zhu, J. M. Glownia, M. E. Kozina, S. Song, S. Nelson, H. Kumazoe, F. Shimojo, R. K. Kalia, P. Vashishta, P. Darancet, T. F. Heinz, A. Nakano, X. Xu, A. M. Lindenberg, and H. Wen, Nat. Photonics **13**(6), 425 (2019).
[14]N. H. Hong, J. Sakai, N. Poirot, and V. Brizé, Phys. Rev. B **73**(13), 132404 (2006).
[15]H. Choi, E. Stathatos, and D. D. Dionysiou, Appl. Catal., B. **63**(1–2), 60 (2006).
[16]W. I. Park, D. H. Kim, S. W. Jung, and G.-C. Yi, Appl. Phys. Lett. **80**(22), 4232 (2002).
[17]P. Umari and A. Pasquarello, AIP Conf. Proc. **677**(1), 269 (2003).
[18]P. Umari and A. Pasquarello, Phys. Rev. Lett. **89**(15), 157602 (2002).
[19]B. Lou, N. Zhao, M. Minkov, C. Guo, M. Orenstein, and S. Fan, Phys. Rev. Lett. **126**(13), 136101 (2021).
[20]P. Kumar, J. Lynch, B. Song, H. Ling, F. Barrera, K. Kisslinger, H. Zhang, S. B. Anantharaman, J. Digani, H. Zhu, T. H. Choudhury, C. McAleese, X. Wang, B. R. Conran, O. Whear, M. J. Motala, M. Snure, C. Muratore, J. M. Redwing, N. R. Glavin, E. A. Stach, A. R. Davoyan, and D. Jariwala, Nat. Nanotechnol. **17**(2), 182 (2022).
[21]D. Lu, D. J. Baek, S. S. Hong, L. F. Kourkoutis, Y. Hikita, and H. Y. Hwang, Nat. Mater. **15**(12), 1255 (2016).
[22]S. Fukushima, S. Tiwari, H. Kumazoe, R. K. Kalia, A. Nakano, F. Shimojo, and P. Vashishta, AIP Adv. **9**(4), 045022 (2019).
[23]I. Souza, J. Iniguez, and D. Vanderbilt, Phys. Rev. Lett. **89**(11), 117602 (2002).
[24]R. Resta, Phys. Rev. Lett. **80**(9), 1800 (1998).
[25]P. E. Blöchl, Phys. Rev. B **50**(24), 17953 (1994).
[26]G. Kresse and D. Joubert, Phys. Rev. B **59**(3), 1758 (1999).
[27]J. P. Perdew, K. Burke, and M. Ernzerhof, Phys. Rev. Lett. **77**(18), 3865 (1996).
[28]J. Fontanella, C. Andeen, and D. Schuele, J. Appl. Phys. **45**(7), 2852 (1974).
[29]M. Schubert, T. E. Tiwald, and C. M. Herzinger, Phys. Rev. B **61**(12), 8187 (2000).
[30]Y. Etinger-Geller, E. Zoubenko, M. Baskin, L. Kornblum, and B. Pokroy, J. Appl. Phys. **125**(18), 185302 (2019).
[31]M. D. Groner, J. W. Elam, F. H. Fabreguette, and S. M. George, Thin Solid Films **413**(1), 186 (2002).
[32]D. A. Buchanan, E. P. Gusev, E. Cartier, H. Okorn-Schmidt, K. Rim, M. A. Gribelyuk, A. Mocuta, A. Ajmera, M. Copel, S. Guha, N. Bojarczuk, A. Callegari, C. D. Emic, P. Kozlowski, K. Chan, R. J. Fleming, P. C. Jamison, I. Brown, and R. Arndt, in the International Electron Devices Meeting 2000, Technical Digest, IEDM (Cat. No.00CH37138) (IEDM, 2000).
[33]S. Jakschik, U. Schroeder, T. Hecht, M. Gutsche, H. Seidl, and J. W. Bartha, Thin Solid Films **425**(1), 216 (2003).
[34]F. Basso Basset, F. Salusti, L. Schweickert, M. B. Rota, D. Tedeschi, S. F. Covre da Silva, E. Roccia, V. Zwiller, K. D. Jöns, A. Rastelli, and R. Trotta, Quantum Information **7**(1), 7 (2001).
[35]M. Upadhyay, M. Ben Elbahri, M. Mezhoud, R. Coq Germanicus, and U. Lüders, Solid-State Electronics **186**, 108070 (2021).

Published under an exclusive license by AIP Publishing